ISSN 1674-1056
http://cpb.iphy.ac.cn
http://iopscience.iop.org/cpb
中国物理 B
Chinese Physics
中国物理
Chinese Physics B

Effects of secondary electron emission on plasma characteristics in dual-frequency atmospheric pressure helium discharge by fluid modeling

Yi-Nan Wang(王一男), Shuai-Xing Li(李帅星), Yue Liu(刘悦), Li Wang(王莉)

Citation: Chin. Phys. B . 2019, 28(2): 025202. **doi:** 10.1088/1674-1056/28/2/025202
Journal homepage: http://cpb.iphy.ac.cn; http://iopscience.iop.org/cpb

What follows is a list of articles you may be interested in

Numerical study on discharge characteristics influenced by secondary electron emission in capacitive RF argon glow discharges by fluid modeling

Lu-Lu Zhao(赵璐璐), Yue Liu(刘悦), Tagra Samir
Chin. Phys. B . 2018, 27(2): 025201. **doi:** 10.1088/1674-1056/27/2/025201

Effects of gas pressure on plasma characteristics in dual frequency argon capacitive glow discharges at low pressure by a self-consistent fluid model

Lu-Lu Zhao(赵璐璐), Yue Liu(刘悦), Tagra Samir
Chin. Phys. B . 2017, 26(12): 125201. **doi:** 10.1088/1674-1056/26/12/125201

Sheath structure in plasma with two species of positive ions and secondary electrons

Xiao-Yun Zhao(赵晓云), Nong Xiang(项农), Jing Ou(欧靖), De-Hui Li(李德徽), Bin-Bin Lin(林滨滨)
Chin. Phys. B . 2016, 25(2): 025202. **doi:** 10.1088/1674-1056/25/2/025202

Characteristics of wall sheath and secondary electron emission under different electron temperatures in a Hall thruster

Duan Ping, Qin Hai-Juan, Zhou Xin-Wei, Cao An-Ning, Chen Long, Gao Hong
Chin. Phys. B . 2014, 23(7): 075203. **doi:** 10.1088/1674-1056/23/7/075203

Characteristics of dual-frequency capacitively coupled SF_6/O_2 plasma and plasma texturing of multi-crystalline silicon

Xu Dong-Sheng, Zou Shuai, Xin Yu, Su Xiao-Dong, Wang Xu-Sheng
Chin. Phys. B . 2014, 23(6): 065201. **doi:** 10.1088/1674-1056/23/6/065201

Effects of secondary electron emission on plasma characteristics in dual-frequency atmospheric pressure helium discharge by fluid modeling*

Yi-Nan Wang(王一男)[1], Shuai-Xing Li(李帅星)[1], Yue Liu(刘悦)[2,†], and Li Wang(王莉)[1]

[1] College of Science, Liaoning Shihua University, Fushun 113001, China
[2] Key Laboratory of Materials Modification by Laser, Ion and Electron Beams (Ministry of Education), Dalian University of Technology, Dalian 116024, China

(Received 9 October 2018; revised manuscript received 2 December 2018; published online 10 January 2019)

A one-dimensional (1D) fluid simulation of dual frequency discharge in helium gas at atmospheric pressure is carried out to investigate the role of the secondary electron emission on the surfaces of the electrodes. In the simulation, electrons, ions of He^+ and He_2^+, metastable atoms of He^* and metastable molecules of He_2^* are included. It is found that the secondary electron emission coefficient significantly influences plasma density and electric field as well as electron heating mechanisms and ionization rate. The particle densities increase with increasing SEE coefficient from 0 to 0.3 as well as the sheath's electric field and electron source. Moreover, the SEE coefficient also influences the electron heating mechanism and electron power dissipation in the plasma and both of them increase with increasing SEE coefficient within the range from 0 to 0.3 as a result of increasing of electron density.

Keywords: dual frequency, secondary electron emission, atmospheric pressure discharge

PACS: 52.50.Dg, 52.50.Qt, 52.65.–y **DOI:** 10.1088/1674-1056/28/2/025202

1. Introduction

It is difficult to control the plasma density and ion energy separately in the radio frequency (RF) capacitively coupled plasma (CCP). However, the dual frequency CCP system is able to achieve separate control of the plasma density and ion bombarding energy.[1–3] The dual frequency CCP system is extensively applied in many fields of materials. In this kind of system, one frequency is chosen to be much higher than the other. The high frequency (HF) source determines the plasma density, and the ion energy depends on low frequency (LF) source.[4,5] Considerable research has been carried out experimentally and theoretically on the dual frequency CCP system for the purpose of improving the efficiency of materials processing.[6–8]

Recently, the dual frequency CCP system has received extensive attention at atmospheric pressure. Many groups have begun to study the characteristics of dual frequency discharge plasmas in many fields to make them attractive for several purposes.[9–12] Waskoening *et al.*[12] studied the plasma ionization and associated mode transitions in dual-frequency helium discharge at atmospheric pressure. Kim *et al.*[13] experimentally studied 13.56 MHz/2 MHz dual frequency in atmospheric pressure corona plasma. Compared with the single frequency plasmas, the gas temperature was nearly same, and there were three discharge modes, positive streamer mode of 2 MHz, negative glow mode of 2 MHz, and continuous glow mode of 13.56 MHz. Zhang *et al.*[14] used a numerical method to study the discharge mode transition and electron heating mechanism in argon dielectric barrier discharge (DBD) driven by dual frequency at atmospheric pressure. They found that the electron energy distribution was effectively modulated by variation of the ratio of the lower frequency component. Liu *et al.*[15] studied the DBD driven by 13.56 MHz/200 kHz dual frequency at atmospheric pressure. They found the RF electric field could improve stability and uniformity at the same time. Despite this research, much of the effects of discharge parameters and the physic processes remain unknown.

The secondary electron emission (SEE) coefficient is an important parameter for material processing technology. As is known to all, the surface properties of materials, a particle's incidence angle and energy will influence the SEE coefficient to some extent. Greb *et al.*[16] studied the impact of changing surface conditions including the SEE coefficient on plasma dynamics and the electron heating. They found that the surface condition significantly influences the characteristics of plasma. Schulze *et al.*[5] studied the secondary electrons in dual frequency capacitive radio frequency discharges. They reported two fundamentally different types of dual frequency at different secondary yields, γ. Shang *et al.*[17] studied the atmospheric pressure RF glow discharge between two

*Project supported by the National Natural Science Foundation of China (Grant No. 11505089).
†Corresponding author. E-mail: liuyue@dlut.edu.cn
© 2019 Chinese Physical Society and IOP Publishing Ltd

coaxial electrodes. They presented that the gas ionization is strongly influenced by SEE coefficient in γ mode. Nevertheless SEE coefficient makes no difference to it in the α mode. Due to an ion's impact on the electrode surfaces, Barkahoum *et al.*[18] reported that the SEE is a significant factor to describe the electrical properties in a discharge. Wei *et al.*[19] used a fluid model to study the influence of secondary electron emission coefficient on dielectric barrier pulsed discharge at atmospheric pressure. They found both the averaged current density in the cathode falling region and the averaged current density in the gap decrease with an increasing SEE coefficient.

In the atmospheric pressure environment, the mechanism of dual frequency discharge has not been fully understood and the fundamental studies are performed rarely. The plasma characteristics depend on the discharge conditions such as electrode distance, gas pressure, driven source, and so on. To simulate different surface conditions, the secondary electron emission coefficient was varied in the model. In some previous works, simple surface conditions of the electrodes are chosen and the effect of SEE is neglected in simulations. In this work, a fluid model including SEE coefficient is used to gain further insight on their fundamental impact on the characteristics of plasma driven by dual frequency in quantitative terms.

2. Model

In this paper, the helium plasma is generated in the parallel-plate electrodes as shown in Fig. 1, where L is the electrode gap. The left electrode is driven by dual frequency source (at $x=0$), and the right electrode is grounded (at $x=L$). The fluid model is used to describe the behavior of plasma by a series of equations including continuity equation, momentum equation and energy equation. In atmospheric pressure discharge, drift-diffusion approximation is used to describe the particle flux instead of momentum equation. The electrode gap is much smaller than the diameter of the electrodes, thus 1D fluid model is adopted. The reactions as same as our previous work of Ref. [20] in helium gas discharge are listed in Table 1. Some assumptions of this model are taken from Ref. [20].

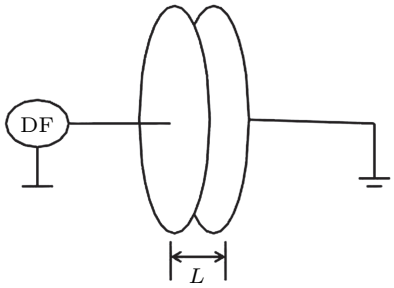


Fig. 1. Schematic diagram of the dual-frequency capacitively coupled plasma reactor.

Table 1. The recantations of helium discharge.

No.	Processes	Coefficient[a)]	H_i/eV	Ref.
1	$e+He \rightarrow He^+ +2e$	$k_1 = 2.584\times10^{-12}T_e^{0.68}e^{(-2.854092\times10^5/T_e)}$	24.6	[22]
2	$e+He \rightarrow He^* +e$	$k_2 = 4.2\times10^{-9}T_e^{0.31}e^{-1.98/T_e}$	19.8	[23]
3	$e+He^* \rightarrow He^+ +2e$	$k_3 = 1.28\times10^{-7}T_e^{0.6}e^{-4.78/T_e}$	4.87	[21]
4	$He^+ +2He \rightarrow He_2^+ +He$	$k_4 = 2.0\times10^{-31}$		[21]
5	$He^* +He^* \rightarrow e+He^+ +He$	$k_5 = 8.7\times10^{-10}$	–15	[21]
6	$He^* +He^* \rightarrow e+He_2^+$	$k_6 = 2.03\times10^{-9}$		[21]
7	$e+He_2^+ \rightarrow 2He$	$k_7 = 4.0\times10^{-9}$		[21]
8	$e+He^* \rightarrow He+e$	$k_8 = 2.9\times10^{-9}$	–19.8	[23]
9	$2He+He^* \rightarrow He+He_2^*$	$k_9 = 1.3\times10^{-33}$		[23]

Units are cm^3/s except for k_9 which is in cm^6/s, The unit of T_e is eV except for k_1 which is in K.

Based on these assumptions the helium discharge can be described as follows. The continuity equation for particles is

$$\frac{\partial n_{e,i,*}}{\partial t}+\frac{\partial J_{e,i,*}}{\partial x}=S_{e,i,*}, \tag{1}$$

where n, J, and S represent density, particle flow density, and particle source term, respectively. And the subscripts e, i, and $*$ denote electron, ion, and metastable, respectively. The drift-diffusion approximation replaces of the momentum equation, thus the particle fluxes can be written as

$$J_{e,i,*}=\mp\mu_{e,i}n_{e,i}E-D_{e,i,*}\frac{\partial n_{e,i,*}}{\partial x}, \tag{2}$$

where μ and D are mobility and diffusion coefficient, respectively, whose values come from Refs. [21]–[23]. E represents electric field. The electron energy equation is

$$\frac{\partial}{\partial t}\left(\frac{3}{2}n_e kT_e\right)=-\frac{\partial}{\partial x}q_e-eJ_e\cdot E-\sum_i H_i k_i n_e N. \tag{3}$$

On the right-hand side of Eq. (3), q_e represents the electron

thermal flow, the second term is the heating term, and the last term is the energy loss term.

$$q_e = -K_e \frac{\partial T_e}{\partial x} + \frac{5}{2} k T_e \cdot J_e, \tag{4}$$

$$K_e = \frac{3}{2} k D_e n_e. \tag{5}$$

Here k is Boltzmann coefficient. e is elementary charge. K_e is the thermal conductive coefficient. H_i denotes the electron energy loss coefficient for ionization.

The Poisson equation satisfies

$$\frac{\partial^2 V}{\partial x^2} = -\frac{e}{\varepsilon_0}(n_i - n_e). \tag{6}$$

The electric field derives from

$$E = -\frac{\partial V}{\partial x}, \tag{7}$$

where the ε_0 is the vacuum permittivity of free space. The initial conditions are

$$n_e = n_i = n_* = 10^7 \text{ cm}^{-3}, \tag{8}$$

$$T_e = 1.0 \text{ eV}, \quad V = 0 \text{ V}. \tag{9}$$

The boundary conditions are as follows:

$$J_e = \pm k_s n_e - \gamma J_i @ x = 0,\ L, \tag{10}$$

$$J_i = -\mu_i n_i \frac{\partial V}{\partial x} @ x = 0,\ L, \tag{11}$$

$$n_* = 0. @ x = 0,\ L, \tag{12}$$

$$T_e = 0.5 \text{ eV} @ x = 0,\ L, \tag{13}$$

$$V = V_H \sin(2\pi f_H t) + V_L \sin(2\pi f_L t) @ x = 0, \tag{14}$$

$$V = 0. @ x = L. \tag{15}$$

Here k_s is the electron surface recombination coefficient calculated assuming an electron sticking coefficient of unity, γ is the secondary electron emission coefficient for ions. $V = V_H \sin(2\pi f_H t) + V_L \sin(2\pi f_L t)$ is the external voltage applied to the left electrode, where the subscripts H and L, respectively, represent the High Frequency (HF) source and Low Frequency (LF) source. We use an implicit center different scheme to solve all of the equations mentioned above.

3. Results and discussion

In this simulation model, helium is chosen as working gas at constant temperature of 300 K. The basic parameters are the background gas pressure $p = 760$ Torr (1 Torr = 1.33322×10^2 Pa) and the electrode distance $L = 0.2$ cm. The voltage of HF source is $V_H = 500$ V and the voltage of the LF source is $V_L = 300$ V. The frequency of the HF source is $f_H = 27.12$ MHz and the frequency of the LF source is $f_L = 2$ MHz. The simulations are performed at different values of γ. The secondary electron emission coefficient is constant for a certain material, based on the experiment and simulation results,[22,24–26] we keep V_H constant and the secondary electron emission coefficients γ within the range from 0 to 0.3. Due to the higher value of V_H at $p = 760$ Torr, the effective acceleration of secondary electrons inside the sheaths leads to a divergence in simulation at the highest values of γ, which would correspond to instabilities or arc formation in an experiment.[5] Thus the highest secondary electron emission investigated is 0.3.

The exactness and suitability of the model was verified by comparing with experimental results. Figure 2 gives the waveforms of applied voltage (solid) and plasma current (dash) in stable discharge stage during two cycles of low frequency. T_L is the cycle of low frequency source. Both the applied voltage and the plasma current are predominately sinusoidal and the current leads the voltage by a phase shift of less than 90°, which are similar to the experimental results of Ref. [27].

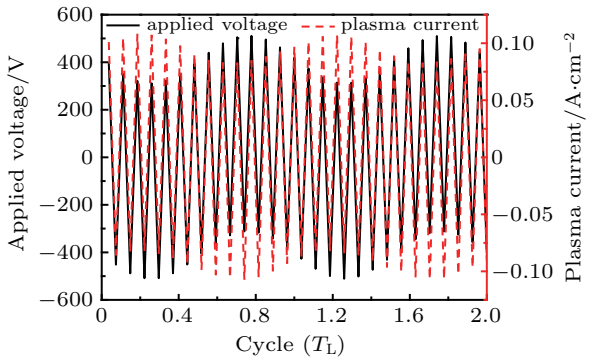


Fig. 2. The waveforms of applied voltage (solid) and plasma current (dash), $V_H = 600$ V, $V_L = 100$ V, $f_H = 27.12$ MHz, $f_L = 2$ MHz.

According to our previous results,[20] the main ions in the atmospheric pressure helium discharge are the He_2^+ ions. Thus, the cycle-averaged spatial distributions of He_2^+ ion are shown in Fig. 3(a) at different SEE coefficients in the 2000th cycle. As the secondary electron emission coefficient increasing from 0 to 0.3, the density of He_2^+ ion increases from 4.3×10^{12} cm^{-3} to 5.7×10^{12} cm^{-3}. The corresponding electron density is shown in Fig. 3(b). The electron density resembles the density of He_2^+ because of the electric neutrality of plasma. It can be clearly seen that the metastable atom He^* density increases as SEE coefficient increasing in Fig. 3(c). The products of metastables are enhanced near the plasma/sheath interface, which results in the peaks of metastable atom He^* density appearing at the same positions on account of higher electron temperature (see Fig. 4(a)). In the bulk plasma metastable pooling (R5 and R6) and step-wise ionization (R3) enhance the losses of metastables, from Table 1, R5 = $k_5 n_* n_*$, R6 = $k_6 n_* n_*$, and R3 = $k_3 n_e n_*$.

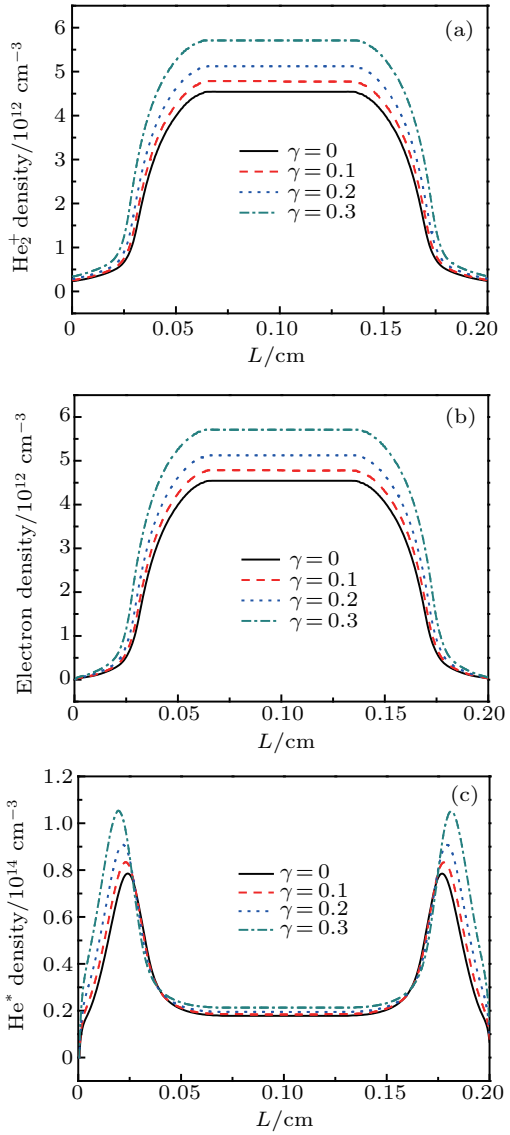


Fig. 3. The profiles of cycle-averaged (a) He_2^+ ion, (b) electron, (c) metastable atom He^* with the SEE coefficient of 0, 0.1, 0.2, and 0.3 in the 2000th cycle, respectively. $V_H = 500$ V, $V_L = 300$ V, $f_H = 27.12$ MHz, $f_L = 2$ MHz.

The cycle-averaged electron temperature and electric field spatial distributions with the SEE coefficient of 0, 0.1, 0.2, and 0.3 in 2000th cycles are shown in Fig. 4. There is a steep gradient near the plasma/sheath interface and the peaks of electron temperature appear at the same positions. In the sheath regions, the electron temperature and electric field increase greatly with the SEE coefficient increasing. However, electron temperature and electric field are almost constant for all SEE coefficients in the bulk plasma. It can be explained that additional electrons from the wall are accelerated and multiplied in the sheath, which increases the number of high energy electrons and the efficiency of multiplication in the sheath. Thus, the sheath becomes smaller and closer to a hard wall because of a higher plasma density. Since the same amount of potential is dropped over a smaller distance, the sheath electric field increases. Although the electron temperature increases greatly with SEE, the thickness of the sheath region reduces very slightly. It because that the thickness of sheath is relevant to density of ions $r_s \propto 1/n_i^{1/2}$. We can see from Fig. 3(a) that the density of ions has changed slightly in the sheath. Therefore, the thickness of the sheath region reduces slightly.

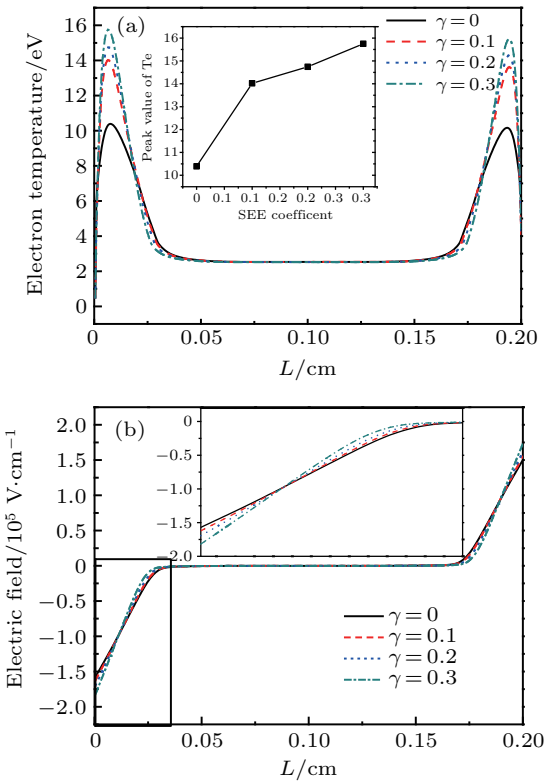


Fig. 4. The profiles of cycle-averaged (a) electron temperature, (b) electric field under different SEE coefficients $V_H = 500$ V, $V_L = 300$ V, $f_H = 27.12$ MHz, $f_L = 2$ MHz.

In low pressure RF discharge, the mechanisms of electron heating are influenced by SEE coefficient.[28–32] In this work, we also focus on the mechanisms of electron heating in dual frequency discharge. Based on the electron energy equation, the mechanism of electron heating $P_C = -eJ_e \cdot E$, labeled as P_C, can be written as:

$$P_C = e\mu_e n_e E^2 + eD_e \frac{\partial n_e}{\partial x} E, \tag{16}$$

$$P_H = e\mu_e n_e E^2, \tag{17}$$

$$P_P = eD_e \frac{\partial n_e}{\partial x} E. \tag{18}$$

Here, P_H and P_P represent the electron ohmic heating and collisionless heating.[28,31] As a result of the inelastic collisions between electrons and neutral particle the electron energy dissipation, labeled as P_L, can be written as

$$P_L = -\sum_i H_i k_i n_e N. \tag{19}$$

The mechanisms of electron heating corresponding to the 2000th cycle in the steady state discharge with different SEE coefficients are shown in Fig. 5. From Fig. 5(a), we can see that the collisionless heating is positive or zero in the bulk

plasma, and it is negative in sheath region. With the SEE coefficient increasing from 0 to 0.3, the peaks of the collisionless heating $P_{\rm P}$ increase in sheath, nevertheless in the bulk plasma the collisionless heating $P_{\rm P}$ has not changed with all the investigated SEE coefficients. This is due to the fact that the important factor is the gradient in the electron density, a greater increase in electron density always occurs in the sheath edge region and the flat shape of electron density in bulk plasma. Figure 5(b) gives the electron ohmic heating with the SEE coefficient varied from 0 to 0.3. The electron ohmic heating mechanism is increasing as the SEE coefficient increased. This is because the electron density increases, which results in the higher conduction current and higher power absorption. Obviously, the electron ohmic heating is dramatically influenced by the SEE coefficient. As the SEE coefficient increases, the electron ohmic heating increases in the whole discharge gap. Figure 5 demonstrates that the secondary electron coefficient influence the electron ohmic heating much more than the collisionless heating. Similar results are found in radio frequency driven capacitively coupled oxygen plasma of Ref. [16], in which both the electron heating mechanisms exhibit a similar increasing trend with increasing secondary electron emission coefficient.

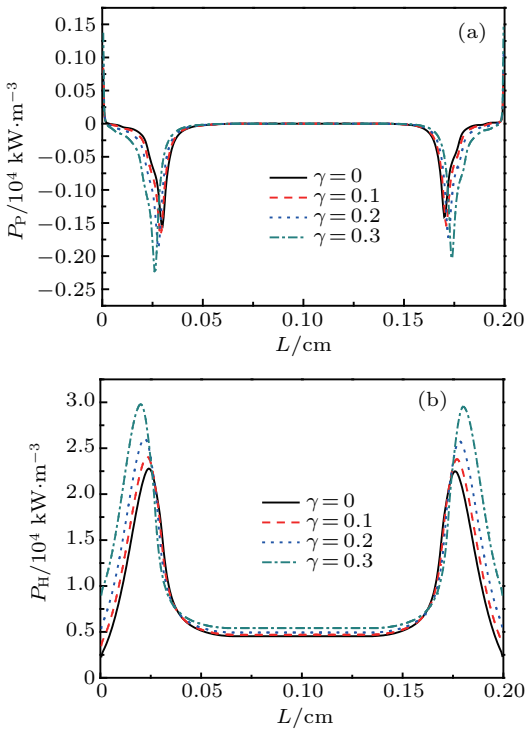


Fig. 5. The cycle-averaged spatial distributions of (a) $P_{\rm P}$, (b) $P_{\rm H}$ with the SEE coefficient of 0, 0.1, 0.2, and 0.3 in the 2000th cycle. $V_{\rm H} = 500$ V, $V_{\rm L} = 300$ V, $f_{\rm H} = 27.12$ MHz, $f_{\rm L} = 2$ MHz.

The electron heating $P_{\rm C}$ corresponding to the 2000th cycle with different electron secondary emission coefficients is shown in Fig. 6. The electron heating $P_{\rm C}$ is the sum of the electron ohmic heating and collisionless heating. Although the collisionless heating is negative in sheath regions, the electron heating $P_{\rm C}$ increases when the SEE coefficient increased due to the higher ohmic heating mechanism. The electron power dissipation is also a main mechanism of discharge and accordingly the electron power dissipation is shown in Fig. 6(b). It is shown that the electron power dissipation increases as the SEE coefficient increased. This is due to the fact that the electron density increases as well. The electron temperature Fig. 4(a) has the similar shape with the electron heating $P_{\rm C}$. Both of them have peaks in the sheath and constant in the bulk. It because the electron energy depends on electrons absorbing energy from the electric field. The electrons absorbing energy from electric field is indicated in the electron heating $P_{\rm C}$. As the SEE increases, the electron density in sheath increases, which results in the sheath of electric field increasing. Thus, both the electron heating and the electron temperature increase in the sheath as shown in Fig. 4(a) and Fig. 6(a). The calculation of the effects of SEE on $P_{\rm P}$, $P_{\rm H}$, $P_{\rm C}$, and $P_{\rm L}$ has a similar tendency to that in low-pressure argon discharge in Ref. [26].

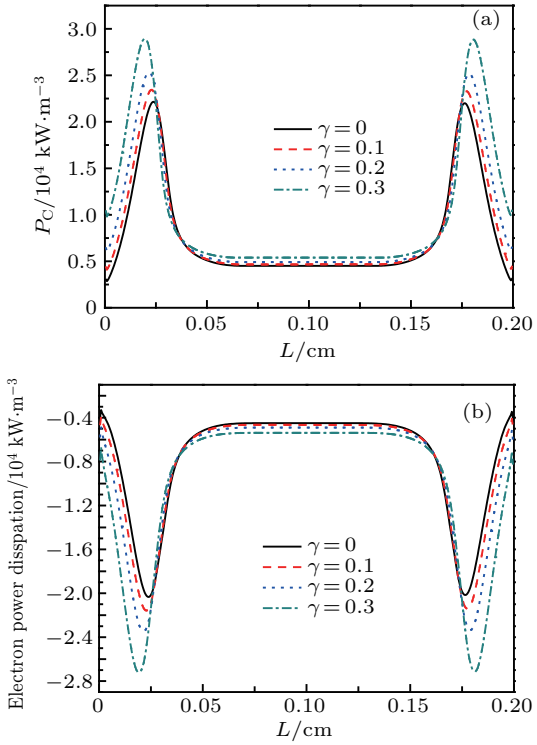


Fig. 6. The cycle-averaged spatial distributions of (a) $P_{\rm C}$, (b) electron power dissipation for different SEE coefficients in the 2000th cycle. $V_{\rm H} = 500$ V, $V_{\rm L} = 300$ V, $f_{\rm H} = 27.12$ MHz, $f_{\rm L} = 2$ MHz.

Figure 7 gives the evolution of electron source $S_{\rm e}$ with different SEE coefficients. The electron source is written as $S_{\rm e} = k_1 n_{\rm e} N + k_3 n_{\rm e} n_* + k_5 n_* n_* - k_7 n_{\rm e} n_{{\rm He}_2^+}$ according to Table 1. We can clearly see that the electron source $S_{\rm e}$ depends on the SEE coefficient. The electron source $S_{\rm e}$ increases as the SEE coefficient increases. The larger the SEE coefficient is, the larger the electron source $S_{\rm e}$ will be. Moreover, the peak region of electron source $S_{\rm e}$ moves to the electrode when the SEE coefficient changes. As the SEE coefficient increases, the sheath thickness decreases, the bulk plasma region enlarges. Besides, the electrons mainly gain energy from sheath's electric field. Consequently the peak of electron source moves as the SEE coefficient changes.

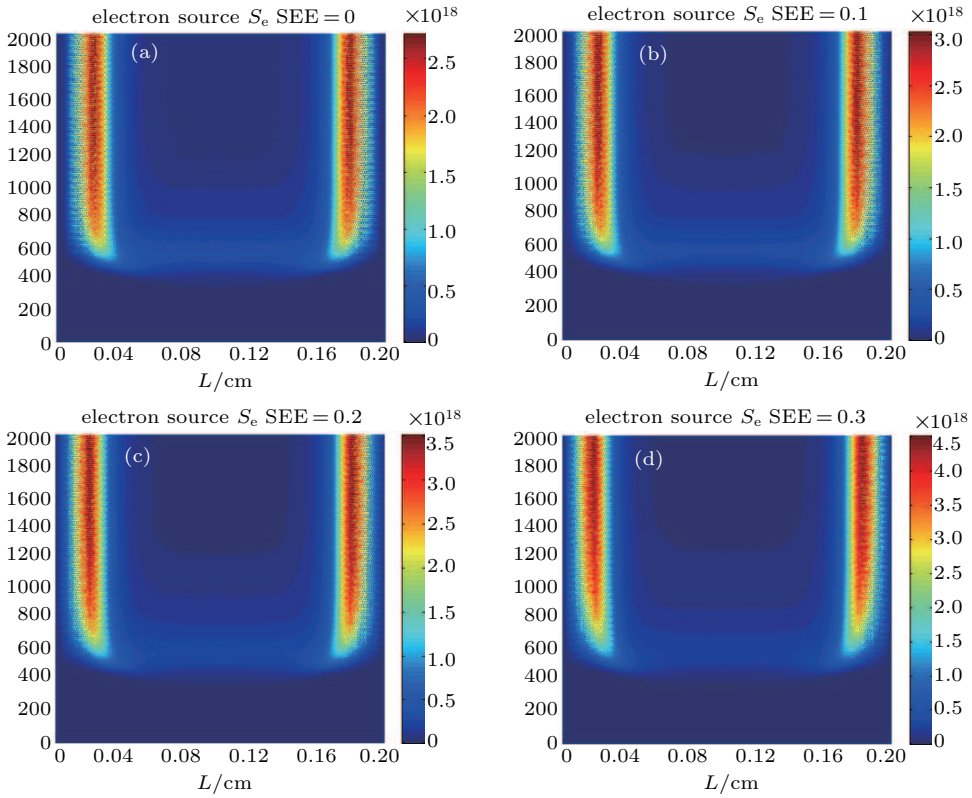


Fig. 7. The evolution of net electron generation with SEE coefficient (a) 0, (b) 0.1, (c) 0.2, and (d) 0.3. $V_H = 500$ V, $V_L = 300$ V, $f_H = 27.12$ MHz, $f_L = 2$ MHz.

4. Conclusion and perspectives

This work studied the effects of secondary electron emission coefficient on the dual frequency helium plasma discharge at atmospheric pressure. The results show that the secondary electrons coefficient has an effect on dual frequency atmospheric pressure helium discharge. It is found that a large SEE coefficient can produce a higher density plasma as well as metastable density, sheath electric field, electron temperature and electron source term. Moreover, the SEE coefficient also influences the electron heating mechanism and electron power dissipation in the plasma and both of them increase with increasing SEE coefficient within the range from 0 to 0.3 as a result of increasing of electron density.

Acknowledgment

We would also extend our thanks to Dr. Li Li for her suggestion and encouragement in this work.

References

[1] Goto H H, Lowe H D and Ohmi T 1993 *IEEE Trans. Semicond. Manufacuring* **6** 58
[2] Booth J P, Curley G, Maric D and Chabert P 2010 *Plasma Sources Sci. Technol.* **19** 015005
[3] Brian G H, Czarnetzki U, Brinkmann R P and Mussenbrock T 2008 *J. Phys. D: Appl. Phys.* **41** 165202
[4] Bi Z H, Xu X, Liu Y X, Jiang X Z, Lu W Q and Wang Y N 2011 *Plasma Sci. Technol.* **13** 181
[5] Schulze J, Donko Z, Schungel E and Czarnetzki U 2011 *Plasma Source Sci. Technol.* **20** 045007
[6] Georgieva V, Bogaerts A and Gijbels R 2003 *J. Appl. Phys.* **94** 3748
[7] Boyle P C, Ellingboe A R and Turner M M 2004 *J. Phys. D: Appl. Phys.* **37** 697
[8] Zhang Z L and Nie Q Y 2015 *The 3rd International Conference on Electric Power Equipment – Switching Technology (ICEPE-ST)*, October 25–28, 2015, Busan, Korea pp. 443–446
[9] Cao Z, Nie Q Y and Kong M G 2009 *J. Phys. D: Appl. Phys.* **42** 222003
[10] Wang Q, Sun J Z, Zhang J H, Ding Z F and Wang D Z 2010 *Phys. Plasma* **17** 053506
[11] Walsh J L and Kong M G 2008 *Appl. Phys. Lett.* **93** 111501
[12] Waskoenig J and Gans T 2010 *Appl. Phys. Lett.* **96** 181501
[13] Kim D B, Moon S Y, Jung H, Gweon B and Choec W 2010 *Phys. Plasma* **17** 053508
[14] Zhang Z L, Lim J W M, Nie Q Y, Zhang X N and Jiang B H 2017 *AIP Adv.* **7** 105313
[15] Liu Y, Peeters F J J, Starostin S A, Sanden M C M and Vries H W 2018 *Plasma Sources Sci. Technol.* **27** 01LT01
[16] Greb A, Gibson A R, Niemi K, O'Connell D and Gans T 2015 *Plasma Scources Sci. Technol.* **24** 044003
[17] Shang W L, Wang D Z and Zhang Y T 2008 *Phys. Plasma* **15** 093903
[18] Larouci B, Bendella S and Belasri A 2018 *Plasma Sci. Technol.* **20** 035403
[19] Yao C W, Ma H C, Chang Z S, Li P, Mu H B and Zhang G J 2017 *Acta Phys. Sin.* **66** 025203 (in Chinese)
[20] Wang Y N, Li S X, Wang L, Jin Y, Zhang Y H and Liu Y 2018 *Plasma Sci. Technol.* **20** 115402
[21] Wang Q, Sun J Z and Wang D Z 2009 *Phys. Plasma* **16** 043503
[22] Zhu X M and Kong M G 2005 *J. Appl. Phys.* **97** 083301
[23] Zhang Y T and Cui S Y 2011 *Phys. Plasma* **18** 083509
[24] Baars-Hibbe L, Sichler P, Schrader C, *et al.* 2005 *J. Phys. D: Appl. Phys.* **38** 510
[25] Hagstrum H D 1960 *Phys. Rev.* **119** 940
[26] Sosov Y and Theodosiou C E 2004 *J. Appl. Phys.* **95** 4385
[27] Huang X J, Dai L and Guo Y, *et al.* 2015 *Phys. Plasma* **22** 103515
[28] Yuan X H and Raja L L 2003 *IEEE Trans. Plasma Sci.* **31** 495
[29] Liu Q, Liu Y, Samir T and Ma Z S 2014 *Phys. Plasma* **21** 083511
[30] Choi E H, Lim J Y, Kim Y G, Ko J J, Kim D I, Lee C W and Cho G S 1999 *J. Appl. Phys.* **86** 6525
[31] Korolov I, Derzsi A, Donko Z and Schulze J 2013 *Appl. Phys. Lett.* **103** 064102
[32] Lafleur T, Chabert P and Booth J P 2014 *Plasma Sources Sci. Technol.* **23** 035010